BMES BIOMEDICAL ENGINEERING SOCIETY

ORIGINAL ARTICLE

Blueprint for a Semi-automated Image Processing Tool to Characterize Stent Features: Application to a Pediatric Growth-Adaptive Stent

Ava E. Giorgianni[1] · Giselle Ventura[2] · Joseph Hollmann[1] · Corin Williams[3]

Abstract

The goal of this work was to develop a general blueprint for a semi-automated image processing tool (SIPT) to measure small, complex features of stent prototypes that can replace the current gold standard of manual measurements. The stents were designed using CAD software and manufactured via laser cutting. Stent prototypes were imaged using a Keyence microscope in top and side view orientations. The SIPT algorithm was developed in MATLAB to extract and measure 4 dimensions of the stent (inner and outer diameter, spring bend outer radius, spring bend width). The same dimensions were also manually measured by an experienced metrology technician as a gold standard comparison. We successfully made over 5000 unique measurements across the 4 key dimensions of 15 stents using the SIPT algorithm. Compared to the gold standard manual method, SIPT reduced measurement time by nearly 90% and increased the total number of measurements captured by over 2300%. The two one-sided test and Bland–Altman analysis demonstrated that SIPT achieved equivalency against the manual method of measurement for all 4 dimensions. In summary, we found that our SIPT software could be used to replace manual measurements and provided substantial time savings with consistent accuracy. Overall, this paper presents a generalizable workflow to isolate and measure critical features of stent prototypes that we believe will provide a valuable, cost-effective tool to other medical device designers seeking to rapidly iterate on unique stent designs or other manufactured parts with small and complex structures.

Keywords Algorithms · Dimension characterization · Stent · Image processing · Quality control

Introduction

Stents are used in a wide variety of healthcare applications [1–4] and the designs must be tailored to meet the requirements of the specific implantation site. The stent market is expected to grow [5] and will require more streamlined tools to detect faulty hardware and guarantee quality of the product. Variations in manufactured stent features, such as

---

geometry and strut thickness, have the potential to drastically impact stent performance [6–8]. The failure of a stent to perform as expected can lead to catastrophic outcomes, particularly in the cardiovascular system. Therefore, a critical first step in quality control is ensuring that stents are manufactured within an acceptable tolerance of the as-designed dimensions. Stents designed for pediatric use or other small anatomical sites are particularly challenging [9] as the designs tend to push the envelope of what is feasible for consistent manufacturing. We are designing a stent for pediatric heart valve replacement with unique features that dictate its growth-adaptive performance [10, 11]. As we and any design team move through R&D phases to scaled-up production, accurate and rapid quality inspection becomes highly desirable.

Currently, the process for quality control of complex hardware is highly manual or requires specialized instrumentation and software, which can introduce high costs, human bias, limitations on production, and operator-to-operator variability. Robust, automated dimensional characterization

methods for manufactured parts have proven key in the development of small-scale technology. Image recognition in the area of production has been rapidly adopted, developed, and implemented across a range of industries [12]. The use of real-time laser scanner cameras and other automated non-contact tools are the norm in the stent industry (e.g., Qualtech, Sensofar Medical). However, these techniques often require costly investment and specialized operators to run the machines. A cost-effective alternative is to utilize commonly available microscopes and software tools to capture, isolate, and measure critical stent features via image processing. The major components of this type of image processing are segmentation algorithms and morphological operations. Segmentation algorithms are built-in to programming language packages like Python and MATLAB and autonomously distinguish between different image regions based on input parameters. These regions are defined by pixel indices which can be used to generate a binary replica of the image. Morphological operations use shapes, called structural elements, to find and utilize pixel patterns in images. These structural elements can be defined by a pre-established shape, such as a disk, rectangle, or line, or by a binary neighborhood of pixels in a complex pattern. We sought to bring the benefits of these semi-automated image processing methods to the production process of stents to ensure accuracy and repeatability while also utilizing low-cost optical imaging capabilities that would be widely accessible to many labs.

Here we present a semi-automated image processing tool (SIPT) to characterize the critical dimensions of a growth-adaptive pediatric heart valve stent without the need for specialized stent imaging equipment. We used a Keyence VHX5000 microscope to acquire images and employed segmentation algorithms and morphological operations to isolate components of interest in the stent images and capture accurate measurements. We present data demonstrating that the SIPT algorithm was equivalent to manual gold standard measurements for 4 important dimensions. We expect that

the work described in this paper will bring the benefits of image recognition to the quality assurance of other stent designs and medical devices with small and complex features. A generalizable workflow from stent design to statistical measurements with key considerations for each step is presented in Fig. 1, and its application is presented in detail for our specific use case of a pediatric stent.

Materials and Methods

Stent Design and Manufacturing

The growth-adaptive pediatric stent design presented as the use case in this work is shown in Fig. 2A. The design requirements for the stent were determined by several key parameters, such as maximum length, functional diameter range, and maximum radial force, which were developed from animal testing data and clinical insights. We measured the dimensions and mechanical properties of pulmonary arteries of juvenile piglets to guide the maximum radial force for tuning our stent performance [13]. Based on clinical reports of pediatric cardiac measurements [14], we chose a functional diameter range of 7 to 14 mm and a maximum stent length of 15 mm [15].

The growth-adaptive stent was designed using a commonly used CAD software, Solidworks® (Waltham, MA), by modeling simple lever arm springs that required minimal material and were able to expand 2-fold. We selected Nitinol as the material for the stent due to its biocompatibility and super-elastic properties [16]. Stents were manufactured by Resonetics (San Diego, CA) using a femtosecond laser, a specialized sizing mandrel, and custom fixturing specific to our stent form factor. The final manufactured stent design for this study consisted of two rows of springs joined by eight equally spaced longitudinal struts (Fig. 2B). In addition, clocking features were created on each strut in order to track stent segments during imaging. The stent had a zero-stress,
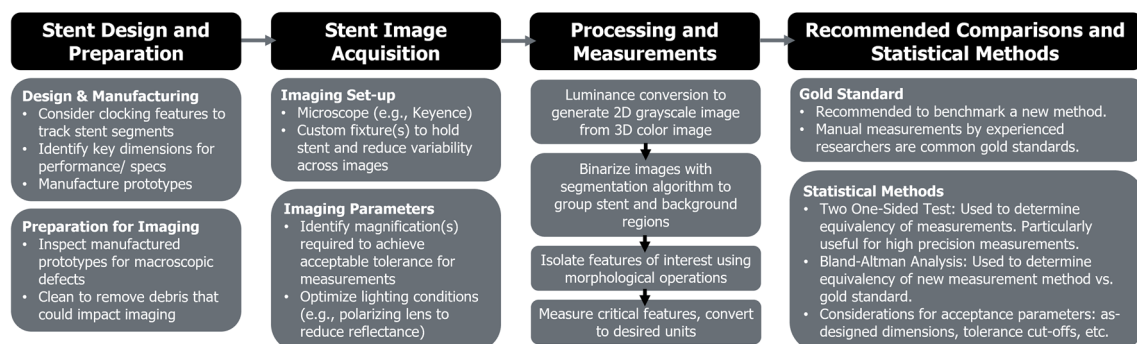
Fig. 1 General workflow for implementing semi-automated characterization of stent design features. Major steps in the workflow are provided at the top (black boxes). Sub-steps and recommendations/best practices are provided below (gray boxes)
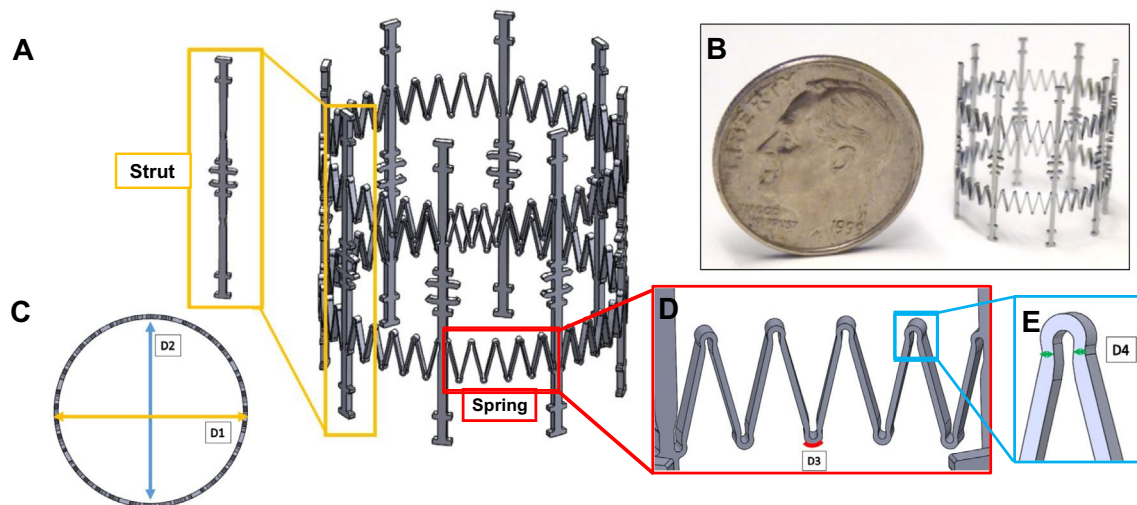
Fig. 2 Pediatric growth-adaptive stent design and key features. **A** Render of the stent with insets showing struts (yellow box) and springs (red box). **B** Manufactured stent with dime for size compar-ison. Key dimensions of interest were **C** [D1] outer and [D2] inner diameter, and **D** spring elements [D3] outer radius and **E** [D4] bend width

fully expanded diameter of 14 mm and was imaged in this configuration.

For this study, we defined 4 key features for semi-auto-mated software detection and measurement. The outer and inner diameters, represented by D1 and D2, respectively (Fig. 2C), were identified as important features as they most clearly demonstrate any plastic deformation that could occur during compression and expansion of the stent during radial force testing or deployment in vivo. Spring bend dimensions D3 and D4 are critical to stent performance as they define the geometry of the spring, and thus the actuating mecha-nism of the stent (Fig. 2D, E).

Stent Preparation and Image Acquisition

A total of 15 stents were manufactured, inspected visually for any gross abnormalities, and cleansed in an ultrasonic bath of isopropyl alcohol to remove debris. The stents then underwent an image acquisition process to capture the 4 dimensions of interest described above using a Keyence VHX5000 (Osaka, Japan) digital microscope (Fig. 3A). A polarizing lens was attached to the microscope lens to reduce specularly reflected light from the surface of the stent and improve contrast in the images for down-stream processing. A custom fixture was 3D-printed to house the stents during side view imaging to reduce movement and increase con-stant alignment (Fig. 3B). For top view imaging, the stent was placed directly on the stage atop a glass insert to allow backlighting (Fig 3C).

Eight side view images were taken per stent, one image for each set of springs between the longitudinal struts, at ×100 magnification with 3D stitching across the *XY* plane,
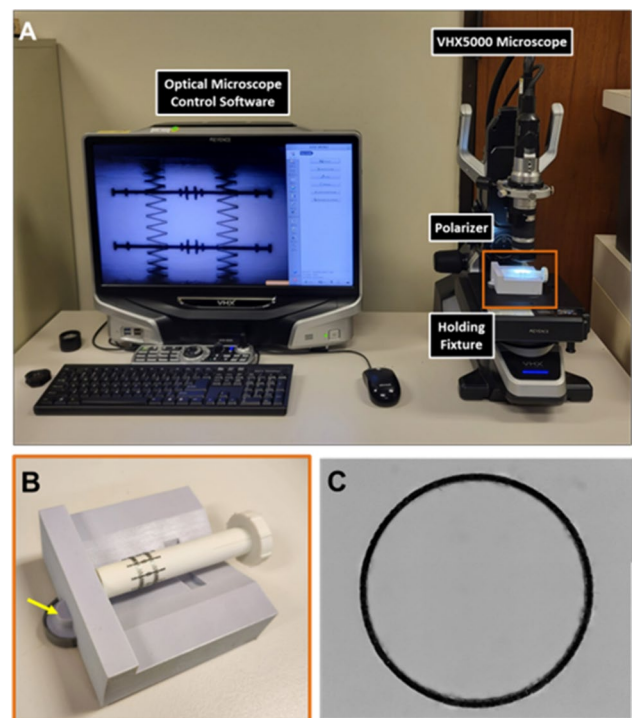
Fig. 3 Imaging set-up and acquisition. **A** Photo of imaging system with key parts labeled. **B** Close-up of stent holding fixture for side view image acquisition. The fixture was designed to maintain a con-sistent orientation of the stent for side view images by inserting the notch on the left (yellow arrow) into a divot on the imaging platform. **C** Representative top view image of the stent (note: side-view is shown on computer screen in **A**

XZ plane, *YZ* planes. Top view images of each stent were taken at ×30 magnification with 2D stitching across the

XY plane. The final dataset for all stents consisted of 120 side view images and 15 top view images. The Keyence was calibrated at each magnification to provide the following measurement conversion factors: 2.3 μm/pixel for the side view images (×100) and 7.6 μm/pixel for the top view images (×30).

Stent Characterization Algorithm

Image Pre-processing

Before isolating and measuring the different components of the stent, the raw stent images were binarized using segmentation algorithms. The 3D color images were first converted to 2D grayscale using a luminance conversion. The grayscale pixel values of the side view images were adjusted to increase the contrast between the stent and the background. Note that this step was unnecessary for the top view images because sufficient contrast was achieved using backlighting during image acquisition. The grayscale images were then used as inputs to built-in MATLAB segmentation algorithms to identify stent versus background regions for binarization.

The side view images were segmented using the fast-marching method [17]. This method requires the user to first identify a small section of the stent using an interactive polygon tool. Then the algorithm utilized the identified positive control pixels and made comparisons to neighboring pixels to isolate the stent from the background. This map was used as a logic array to create a binarized image of the stent. A fill operation was then applied to the binarized side view images to ensure all components of the stents were continuous. Finally, a morphological erosion using a disk structural element was applied to the images to counteract the dilation that occurs during segmentation (Fig. 4A).

The top view images were segmented using the k-means clustering method [18]. The algorithm autonomously defined two distinct regions, stent and background, by iteratively calculating the centroids of each established region and providing a labeled matrix indicating which pixels belonged to which region. The image was cropped prior to segmentation to remove edge artifacts. After segmentation, a median filter and morphological opening operation were applied to the binarized top view images to smooth the regions and remove noise.

Characterization of Side View Stent Features

The features of interest in the side view images were the bends of the springs, which were characterized largely by two key dimensions: (D3) outer radius and (D4) bend width. The bends were isolated through a series of morphological operations applied to different components of the stent (Fig. 4B).

The binarized side view images were first cropped at the struts. Pixel row coordinates for the crop were obtained by isolating the struts using line structural elements in a morphological opening. The orientation of the line structural elements was swept from −1 to 1 degrees in 0.5-degree increments and the length of the line structural elements was set to roughly the as-designed length of the strut, 15 mm. The angle sweep was implemented to account for potential misalignment of the stent in the image. Morphological
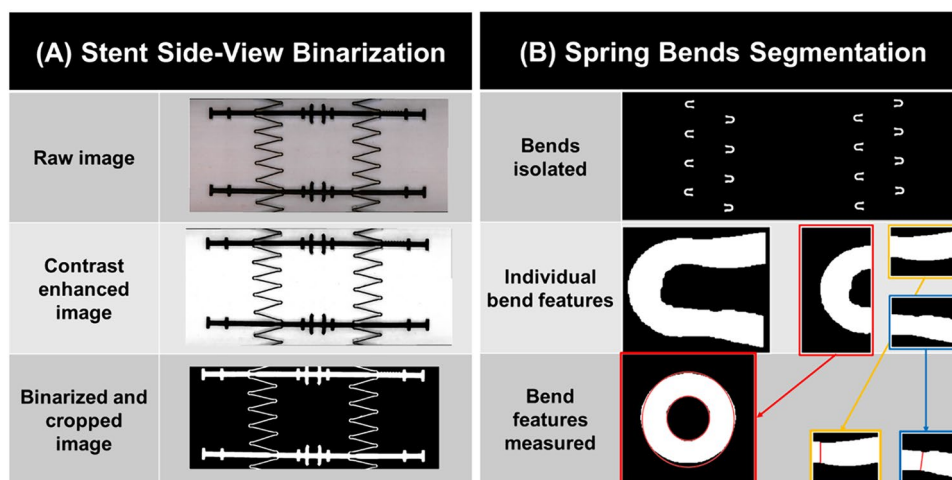
Fig. 4 Image processing workflow for side-view binarization and small bend isolation and measurement. **A** The raw image was contrast enhanced and then used as an input to the segmentation algorithm. The two distinct regions isolated during segmentation were used to produce a binarized representation of the image. **B** The isolated bends were measured individually. Each bend was cropped at the center point of the curve, which was then reflected to create a circle and measure the outer radii. The 2 bend segments per spring were measured at the smallest width, represented by the vertical red lines

opening was conducted in a loop using a line structural element at each orientation in the angle sweep. The binary output of the operation that best preserved the struts, which was determined by which output had the greatest sum of pixels, was selected to determine crop coordinates. This step was important to eliminate support features in the stent that do not require measurement.

Once the binary image was cropped to exclude the struts, the spring segments were isolated and removed from the image. Line structural elements were once again used in a morphological opening, this time with the length set to about 0.5 mm and the angle set to 0 degrees to capture the horizontal width of the spring segments but not the tips of the small bends. From the spring segment end points, the column indices were extended inward ~ 1 mm and everything between the two indices was set equal to zero to eliminate the spring segments and preserve the bends. Each isolated bend was then identified and labeled as a connected component of the image using an object identification algorithm.

For the outer radii of the bends (D3), the bend was reflected at its center point to create a full circle (Fig. 4B, red box). The algorithm counted the number of pixels horizontally and vertically across the circle, took the average, and divided by two. Small bend width measurements (D4) were calculated by utilizing pixel indices along the borders of the individual isolated bends. The top and bottom segments of the other half of the bend (Fig. 4B, blue and yellow boxes) were separated with cropping, and the minimum distance in pixels across those sections of the bend was taken as the bend width measurement (2 per spring bend). The measurements in pixels were then converted to mm using the conversion factor specified by the Keyence for the side view images at ×100 magnification.

Characterization of Top View Stent Features

The two critical dimensions obtained from the top view images of the stents were the (D1) outer and (D2) inner diameters. The minimum Feret distances of the binarized top view images and the image complements were taken, which corresponded to the outer and inner diameters of the stent, respectively, in pixels. The minimum Feret distance was used rather than the maximum to avoid faulty measurements from potential segmentation artifacts. The measurements in pixels were converted to mm using the conversion factor specified by the Keyence for the top view images at ×30 magnification.

Manual Metrology Measurements

Manual measurements of the 4 key dimensions were made on 5 of the manufactured stents by an experienced metrology technician using the Keyence dimensioning software.

These metrology measurements served as the gold standard comparison for the SIPT algorithm.

Statistical Analyses

A primary goal of our study was to determine whether the SIPT algorithm could be used as a replacement for the gold standard manual measurements. We used two different statistical approaches to compare measurements between the two methods from a subset of 5 stents. Specifically, we conducted a two one-sided test (TOST) [19] and Bland–Altman analysis [20] to test for equivalency. The upper and lower bounds for TOST were determined by the difference between the as-designed dimensions and the averages of the gold standard metrology measurements. Our rationale was that actual measured deviation, within reason, away from the as-designed dimension should be acceptable, as we do not expect all manufactured parts to be exactly equivalent to the as-designed specifications. For Bland–Altman analysis, we used the percent difference vs. average method to determine the bias and limits of agreement between the two methods of characterization. For Bland–Altman, the mean value for each of the 4 dimensions was used for the $N = 5$ stents in which both measurement methods had been applied.

Results

As described above in the methods, we focused on 4 dimensions that we deemed critical to our pediatric stent design to be measured in this study (Fig. 2). Images of 15 stents were captured and measured with the SIPT software using the Keyence set-up illustrated in Fig. 3 and image processing workflow of Fig. 4. Of the 120 side view images, 116 (96%) were successfully segmented with the algorithm. Of the 15 top view images, 13 (87%) were successfully segmented with the algorithm. Images from stents 1-5 were measured manually using a metrology tool as the gold standard method for comparison to the SIPT algorithm. The aggregate data for the 4 dimensions across all stents measured (15 for SIPT, 5 for metrology) are shown in Figs. 5 and 6.

The outer diameter (D1) and inner diameter (D2) of the stent captured by the two measurement methods are compared using box plots in Fig. 5. The box plots show that the data spread for both methods cover similar measurement ranges in both dimensions. All data falls under the as-designed dimension lines, marked at 14 mm and 13.4 mm, respectively, with the difference on the order of ~ 300 to 500 μm. Figure 6 compares the spread of the spring bend measurement data between the two methods, visualized in histograms, showing normal distribution for both SIPT and metrology. Both D3 and D4 had a high amount of overlap
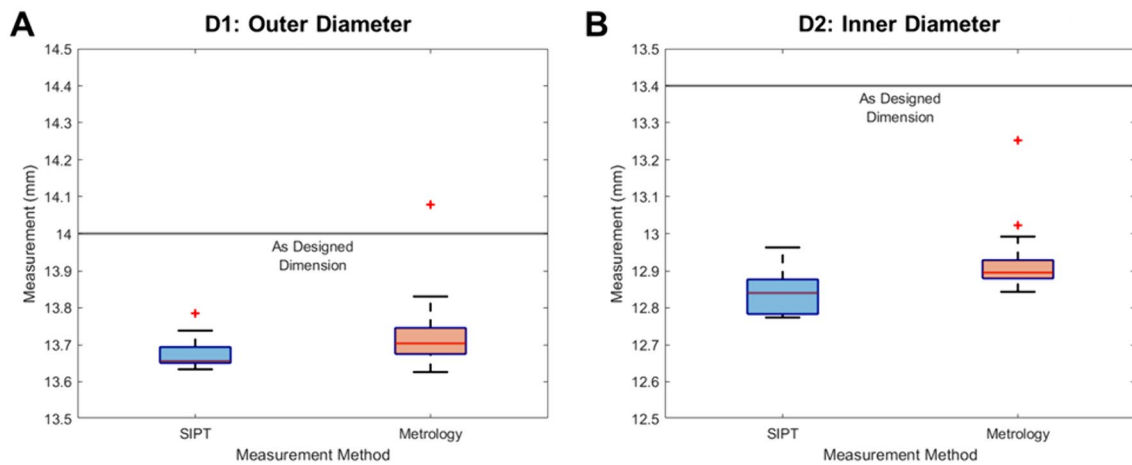
Fig. 5 Box plots of stent top view measurements. **A** Outer diameter and **B** inner diameter, for the SIPT (blue) and metrology (orange) methods. The as-designed dimension is indicated by the horizontal black line. $N=26$ total top view measurements for SIPT and $N=30$ total top view measurements for metrology. Graphs created using MATLAB
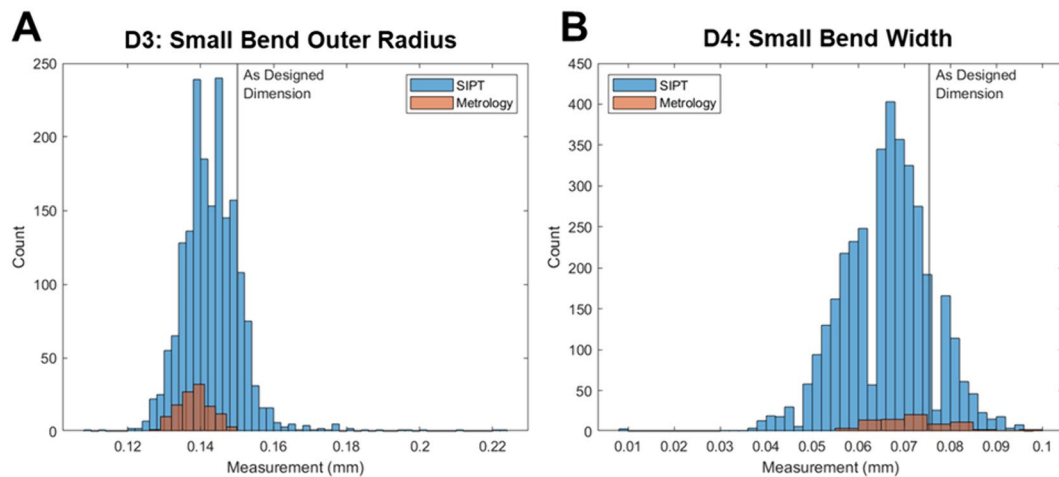
Fig. 6 Histograms of spring bend measurements. **A** Outer radius and **B** bend width for the SIPT (blue) and metrology (orange) methods. The as-designed dimension is indicated by the vertical black line. Total side view measurements are $N=5522$ for SIPT (15 stents) and $N=199$ for metrology (5 stents). Graphs created using MATLAB

between the SIPT and metrology methods and showed good agreement with as-designed dimensions.

The above trends were consistent when analyzing the individual scatterplots for all 15 stents measured with the SIPT algorithm. Across stents, there was not a substantial amount of variation in the range of measurements, and all 15 stents showed good agreement with as-designed value, indicating reasonable consistency in manufacturing of the complex bend features. When comparing on a stent-by-stent basis for the 5 stents measured by both SIPT and metrology, there was clear agreement between the majority of the SIPT and metrology data in D3 and D4, with heavy overlap of the interquartile ranges for nearly every stent (Supplementary Fig. 1).

The data collected through both the gold standard metrology and SIPT measurements have tight standard deviations due to the nature of the dimensions. To assess whether the SIPT measurements were equivalent to metrology, a series of two one-sided tests of each dimension were conducted with a 95% confidence interval, with the upper and lower bounds for each dimension determined by the difference between the gold standard mean for metrology and the as-designed dimension, as described in the methods. The SIPT measurements for all 4 dimensions were found to be equivalent with the metrology measurements (Table 1). The Bland–Altman test also indicated good agreement between the two methods for each dimension, which typically ranged < 6% difference and only exceeded 10% difference for the mean

Table 1 Equivalency test for SIPT and metrology methods

|	95% CI (Mean SIPT—Mean Met)	Equivalence Interval	Equivalent
D1	− 0.1666, 0	± 0.561	Y
D2	− 0.1388, 0.01133	± 0.324	Y
D3	0, 0.005670	± 0.0069	Y
D4	− 0.007271, 0	± 0.0092	Y

Results of TOST statistical analysis

measurements of D4 on 2 stents (Fig. 7). When comparing the percent difference from the as-designed dimensions, both SIPT and metrology showed < 10% difference with the exception of SIPT D4 (Table 2).

The SIPT algorithm was capable of performing analysis of the 2 top view dimensions in 13.1 s on average and all instances of the 2 side view dimensions in 39.6 s on average, based on a sample of 8 side view images. This resulted in

an average total measurement time of around 330 s (~ 5.5 min) per stent for the software. Given that the time required to manually measure only 2–3 instances of each key dimension per stent section was estimated at about 1 h per stent, the total analysis time per stent was reduced by more than 90% using the software. Considering there are 16 instances of D3 and 32 instances of D4 per stent segment and 8 segments per stent, we estimated that manually measuring each instance of all 4 key dimensions would take at least 6 hours of manual labor per stent. Overall, SIPT provided a dramatic increase in the number of measurements with a similarly drastic reduction in time, as summarized in Table 3.

Discussion

The goal of our study was to develop a consistent and automated quality control software tool to measure critical, complex features of pediatric heart valve stents without the need
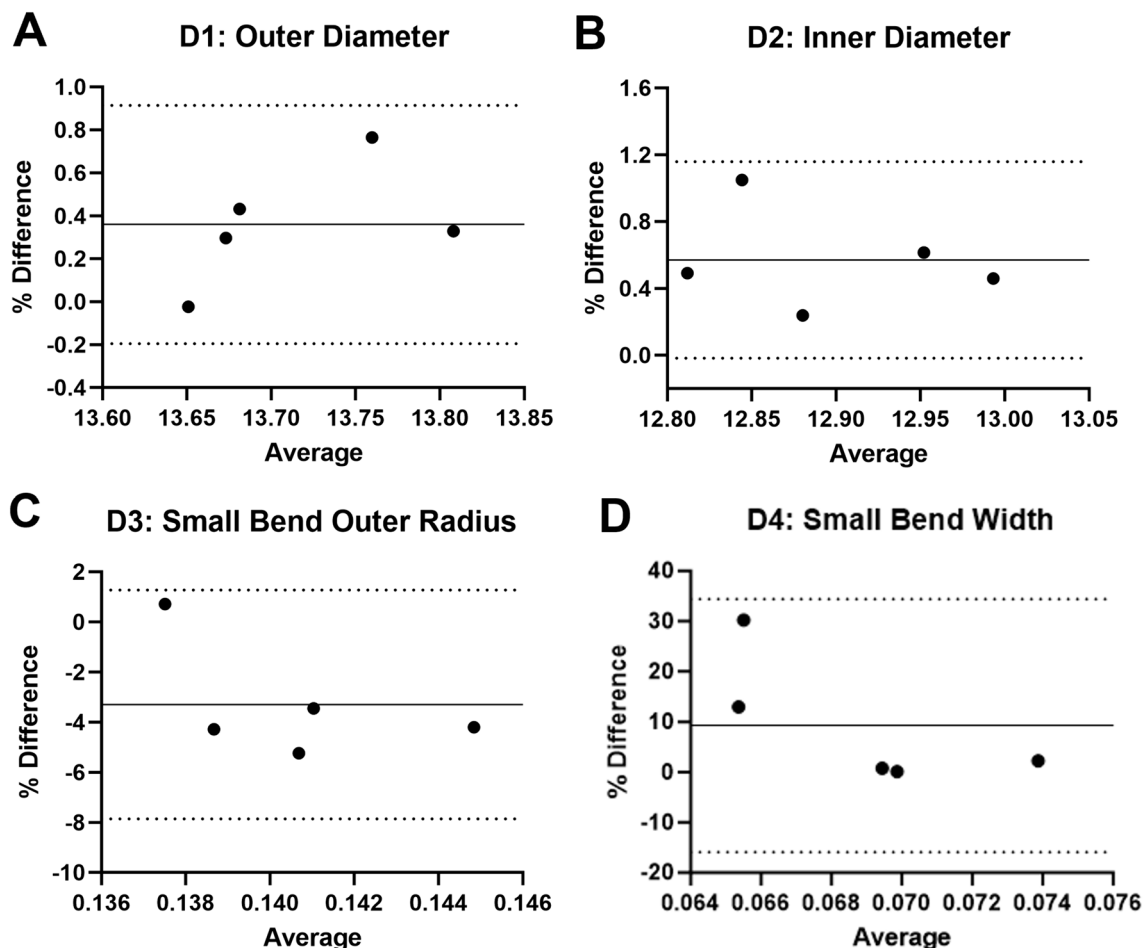
Fig. 7 Bland–Altman agreement analysis comparing the SIPT and metrology methods for all 4 dimensions. Mean values for each dimension of the 5 stents, measured by both SIPT and metrology, were used to calculate the percent difference. Solid lines indicate the bias and outer dashed lines indicate the limits of agreement (± 1.96 SD). Graphs created using GraphPad Prism

Table 2 Percent difference from as-designed dimensions

Dimension	Metrology (%)	SIPT (%)
D1	1.9	2.3
D2	3.6	4.3
D3	8.2	4.7
D4	4.9	13.0

The means of each dimension dataset were used to calculate percent differences

Table 3 Number of measurements capture and time required

Method	Measurements per stent	Estimated time per stent (s)
Metrology	42	3600
SIPT	386	330

for time-intensive manual measurements. Our stent characterization approach achieved a drastic reduction in time while preserving the accuracy of measurements via a fast, semi-automated algorithm. We utilized a readily available imaging system, the Keyence VHX5000, with a custom 3D printed fixture and polarizing lens to ensure consistent image acquisition and quality of our samples. The SIPT algorithm developed in MATLAB applied image segmentation and processing techniques to isolate and measure different features of the stent. The measurements produced from the SIPT algorithm were statistically equivalent to those provided by the manual metrology measurement gold standard as determined by TOST and Bland–Altman statistical analyses. This new capability will facilitate streamlined quality evaluation of our manufactured stents, allowing us to move rapidly into further testing, both ex vivo and in vivo. More broadly, the approach described in this work provides a blueprint that can be adapted to other imaging platforms and software as available to stent and medical device design community. Images of various manufactured parts with small, complex, or otherwise difficult to measure features could be analyzed using an adapted version of this process, following the guiding principles in the workflow in Fig. 1. Further discussion of best practices is provided below.

Stent Design and Preparation

A critical first step is identifying which stent features are important to characterize. These features should be tied to performance parameters of the stent. Stent diameter, wall thickness, strut length and/or width, and spring elements are examples of features that are typically important to stent performance or other design specifications. For repeated structures, such as the spring elements in our pediatric stent, we suggest including clocking features in the design to map the acquired images to specific stent segments. Manufactured prototypes should be visually inspected and cleaned prior to high resolution imaging to streamline the quality control process.

Stent Image Acquisition

First, feature size and features of interest have to be taken into consideration when refining the image acquisition process. For our side view images, the features of interest (spring bends) were substantially smaller than the stent diameter captured in the top view (µm-scale vs. mm-scale), hence our decision to use ×100 magnification for side view images and ×30 magnification for top view images. It is important to note the magnitude of your features of interest and the tolerance of the machine measurements at each magnification. Higher magnification objectives can capture small dimensions with more accuracy, but often take longer to acquire, for example, if the images must be stitched for a region of interest. One must consider the balance between the resolution required and speed of image acquisition. It is also important to consider 2D stitching vs 3D, particularly in the context of stents. 3D stitching is valuable for keeping features in focus across a range of distances in the z-plane (e.g., in side view imaging in which there is curvature in the stent), but is more time consuming than 2D stitching. 2D stitching is best for flat components or features of interest along the same z-plane (such as the top view of our stents).

Additionally, lighting parameters can have a substantial impact on image quality and down-stream processing. A full ring light provides consistent illumination on the target. Backlighting reduces detail visible on the front features but can help create clear distinction between stent and non-stent regions of the image. This was our rationale for utilizing backlighting for our top view images. We also used a polarizing lens to reduce reflection off the metallic stent surface and improve contrast in the images. In general, it is important to keep in mind the critical features to be analyzed and select lighting conditions that enhance contrast between the background and the stent. High contrast enables the segmentation algorithms to identify the region of interest more precisely and successfully isolate the stent in the image.

Processing and Measurement

While we applied SIPT to specific stent features, the general approach presented in the workflow (Fig. 1) can be adapted to other stent measurements. The structural elements and morphological operations will be the main customizable portions of the algorithm. The image resolution, directly related to the magnification used for image acquisition, will

determine the size of the structural elements required to isolate the features of interest. The Keyence machine provided a pixel-to-mm conversion factor which we used to determine the dimensions, in pixels, of structural elements used to isolate the stent features. Structural element shape, size, and orientation are all key to successfully isolating device components of interest in the software and can be tuned for different stent designs.

Statistical Methods and Comparisons

When developing a new measurement methodology, it is best practice to compare its equivalency to a gold standard method as the "ground truth". This approach is common in clinical and pharmaceutical research [19, 20]. We used TOST and Bland–Altman analyses to determine whether the SIPT algorithm was equivalent to the gold standard manual measurements made by an experienced metrology technician. Note that these statistical methods were intentionally selected for determining *equivalence*, as opposed to the commonly used Student *t*-test or ANOVA for determining significant *differences* between measurements or experimental groups. TOST is particularly useful for methods which require high precision, such as the measurement of small features of stents manufactured with tight tolerances. The implementation of TOST and Bland–Altman provides flexibility to the researcher to define acceptable limits, but note that the acceptance criteria should be defined a priori and have clear rationale. For example, we determined the upper and lower bounds for TOST as the difference between the as-designed dimensions and the average gold standard manual measurements to provide for some expected variation in the manufactured dimensions within reasonable tolerance.

Despite the success of the algorithm, we recognize some sources of error and limitations. First, there were discrepancies in the measured and as-designed dimensions, even with the gold standard. We believe this is likely due to variations in manufacturing and do not reflect inaccuracy in the measurements themselves. In addition, there was a ± 3 pixel tolerance for measurements obtained by the Keyence microscope employed in this study. This pixel tolerance indicates that measurements at lower resolutions, namely the ×30 top view images, have a wider margin of error. Specifically, the tolerance for measurements in the ×30 magnification top view images was ± 23 μm and for 100x side view images was ± 6.9 μm. These margins of error affect both the metrology and SIPT data since both use the Keyence pixel-to-mm conversion factor. We argue that this potential error is negligible for the top view measurements, since the ×30 tolerance is only 0.18% of the smallest top view dimension, D2. However, the error potentially becomes more significant in the side view images, as the ×100 tolerance is 10.4% of the smallest side view dimension, D4. We note this is a limitation of the

imaging system we currently have available; in future work we could increase imaging power beyond ×100 magnification. Nevertheless, our SIPT algorithm achieved sufficient accuracy to meet the primary objectives of increasing the number of measurements made in a time-efficient manner while maintaining accuracy compared to the gold standard manual method. Overall, the SIPT algorithm shows high potential for rapid, reliable, large-scale quality assurance of stents with small and complex design features.

In conclusion, we found that our semi-automated measurement software demonstrated equivalence to the gold standard manual method for all 4 dimensions measured, provided overall analysis time reduction by more than 90% with consistent accuracy, and shows promise for continued development towards further stent feature characterization. The stent measurement approach presented here provides a valuable tool for stent quality control, which can be generalized for medical device designers in the R&D phase seeking to rapidly iterate on unique and novel stent designs. With further development, SIPT can be enhanced and transitioned into a fully automated imaging platform that can accommodate various types of stents or other medical devices with small and complex features.

Declarations

Competing Interests The authors declare that they have no conflicts of interest.

References

1. Pan, C., Y. Han, and J. Lu. Structural design of vascular stents: A review. *Micromachines (Basel)*. 12(7):770, 2021. https://doi.org/10.3390/mi12070770.
2. Johnson, C. M., A. S. Luke, C. Jacobsen, N. Novak, and G. R. Dion. State of the science in tracheal stents: A scoping review. *Laryngoscope*. 132(11):2111–2123, 2022. https://doi.org/10.1002/lary.29904.

3. Bernasconi, V., et al. Comprehensive overview of ureteral stents based on clinical aspects, material and design. *Cent Eur. J. Urol.* 76(1):49–56, 2023. https://doi.org/10.5173/ceju.2023.218.

4. Li, L., X. Zhang, Y. Chen, H. Wan, F. J. Herth, and F. Luo. Airway stents from now to the future: a narrative review. *Respiration.* 102(6):439–448, 2023.

5. Linu, D., and S. Onkar. Stents market size, share | Growth Prediction – 2030. Market research, 2021. Accessed Oct. 14 2023. https://www.alliedmarketresearch.com/stents-market

6. Shen, X., H. Yi, and Z. Ni. Effects of stent design parameters on radial force of stent. in *2008 2nd International Conference on Bioinformatics and Biomedical Engineering*, May 2008, pp. 1712–1716. https://doi.org/10.1109/ICBBE.2008.756.

7. Matsumoto, T., et al. Radial force measurement of endovascular stents: Influence of stent design and diameter. *Vascular.* 24(2):171–176, 2016.

8. Wang, Q., G. Fang, Y.-H. Zhao, and J. Zhou. Improvement of mechanical performance of bioresorbable magnesium alloy coronary artery stents through stent pattern redesign. *Appl. Sci.* 8(12):2461, 2018.

9. Peters, B., P. Ewert, and F. Berger. The role of stents in the treatment of congenital heart disease: Current status and future perspectives. *Ann. Pediatr. Cardiol.* 2(1):3–23, 2009. https://doi.org/10.4103/0974-2069.52802.

10. King, D. F., S. L. Golmon, R. Coppeta Jonathan, M. Carr Jesse, C. Williams, Corin. Growth adapative expandable stent

11. Feins, E. N., and S. M. Emani. Expandable valves, annuloplasty rings, shunts, and bands for growing children. *Semin. Thorac. Cardiovasc. Surg.* 23:17–23, 2020. https://doi.org/10.1053/j.pcsu.2020.02.002.

12. Babic, M., M. A. Farahani, and T. Wuest. Image based quality inspection in smart manufacturing systems: A literature review. *Procedia CIRP*. 103:262–267, 2021. https://doi.org/10.1016/j.procir.2021.10.042.

13. Sutherland, D. W., et al. Characterization of main pulmonary artery and valve annulus region of piglets using echocardiography, uniaxial tensile testing, and a novel non-destructive technique. *Front. Cardiovasc. Med.* 9:884116, 2022. https://doi.org/10.3389/fcvm.2022.884116.

14. Beekman, R. H., et al. Pathways to approval of pediatric cardiac devices in the United States: challenges and solutions. *Pediatrics.* 124(1):e155-162, 2009. https://doi.org/10.1542/peds.2008-3726.

15. Hofferberth, S. C., et al. A geometrically adaptable heart valve replacement. *Sci. Transl. Med.* 12(531):4006, 2020. https://doi.org/10.1126/scitranslmed.aay4006.

16. Wadood, A. Brief overview on nitinol as biomaterial. *Adv. Mater. Sci. Eng.* 2016:e4173138, 2016. https://doi.org/10.1155/2016/4173138.

17. RoyCardinal, M.-H., J. Meunier, G. Soulez, É. Thérasse, and G. Cloutier. Intravascular ultrasound image segmentation: a fast-marching method. In: Medical Image Computing and Computer-Assisted Intervention-MICCAI 2003. Lecture Notes in Computer Science, edited by R. E. Ellis, and T. M. Peters. Berlin: Springer, 2003, pp. 432–439. https://doi.org/10.1007/978-3-540-39903-2_53.

18. Dhanachandra, N., K. Manglem, and Y. J. Chanu. Image segmentation using K-means clustering algorithm and subtractive clustering algorithm. *Procedia Comput. Sci.* 54:764–771, 2015. https://doi.org/10.1016/j.procs.2015.06.090.

19. Limentani, G. B., M. C. Ringo, F. Ye, M. L. Berquist, and E. O. McSorley. Beyond the *t*-test: Statistical equivalence testing. *Anal. Chem.* 77(11):221A-226A, 2005. https://doi.org/10.1021/ac053390m.

20. Bland, J. M., and D. G. Altman. Statistical methods for assessing agreement between two methods of clinical measurement. *Lancet.* 1(8476):307–310, 1986.